Journal of Electrical Systems and Information Technology

RESEARCH Open Access

Performance and security enhancement using generalized optimal unified power flow controller under contingency conditions and renewable energy penetrations

K. V. Kumar Kavuturu[1*], K. N. V. Sai Tejaswi[1] and Varaprasad Janamala[2]

*Correspondence:
vasishta.kavuturu@gmail.com

[1] Vijayawada , Andhra Pradesh 521212 , India
[2] Department of Electrical and Electronics Engineering, School of Engineering and Technology, Christ (Deemed to be University), Bengaluru, Karnataka 560074, India

Abstract

In this paper, a novel flexible AC transmission system (FACTS) device named generalized optimal unified power flow controller (GOUPFC) is introduced to control the power flows in multi transmission lines and to regulate the voltages and angles at the load buses. The detailed power injection modeling of GOUPFC is presented in this paper. The optimal location of GOUPFC is determined based on line collapse proximity indicator (LCPI). A multi-objective function is framed in terms of average voltage deviation (AVDI), real power loss (P_{loss}) and average line collapse proximity indicator ($LCPI_{avg}$) to test the effectiveness of the proposed device. The simulation studies are performed on standard IEEE 57-bus test system under single line contingency and considering various renewable energy source (RES) penetrations. The control parameters of GOUPFC are optimized by using whale optimization (WO-BAT) algorithm, by hybridizing WOA and BAT algorithms, and the superiority of WO-BAT is observed in minimizing the proposed objective function and enhancing the voltage profile.

Keywords: Average voltage deviation (AVDI), Generalized unified power flow controller (GUPFC), Phase shifting transformer (PST), Optimal power flow (OPF), Whale optimization-BAT (WO-BAT)

Introduction

The growing threat of global warming has spurred the integration of various renewable energy (RE) technologies into various power systems. In addition to its advantages for the environment, intermittent sources of energy can cause a lot of problems with power quality [1]. The development of novel AC-DC hybrid systems with energy storage and the deployment of power quality controllers like FACTS devices can help resolve these problems [2]. In the literature, numerous researchers have concentrated on the application of FACTS devices on enhancing steady-state stability and power system performance under varied probable situations. However, a few studies are only concerned with their efficient management of RE uncertainties. To tackle line contingencies and RE uncertainties, this research introduces an innovative and sophisticated FACTS device.

The evolution of FACTS technology in the power system industry is employed in demand control, voltage stability and control, active and reactive power flow control, improving quality and conditioning of power in transmission system, power factor correction, voltage regulation, minimizing the real and reactive power losses, reactive power compensation; enhances the transmission system security, enhancement of transient and steady-state voltages; and finally reduces the installation cost of the transmission system due to expansion demanded by the load [3–5]. Also, the progressions in the technology advancement new concepts and strategies are introduced in the FACTS devices in the last two decades. The detailed literature review on the existing FACTS devices is found in [6]. UPFC is the basic second-generation FACTS device which regulate the bus voltages and phase angles and control the power flow in all the lines of the power system. The reformed version of UPFC is GUPFC, which can do the same function of UPFC but in multiple lines. The detailed mathematical modeling of GUPFC with three converters in nonlinear interior optimal power flow is implemented in [7]. A hybrid approach for GUPFC optimal location is implemented to damp out inter-area oscillations which is proposed in [8]. Transient stability margin is improved with neuro-fuzzy controller for GUPFC device by damping out transient oscillations and is implemented in [9]. The superiority of GUPFC over M-UPFC for enhancing voltage profile and improving power flow is observed in [10]. The power quality improvement in terms of reducing total harmonic distortion level with a 72-pulse VSC based GUPFC is presented in [10]. The demand-side congestion cost is increased if more number of lines in a transmission system are congested and this cost estimated with and without GUPFC device and observed the cost reduction with GUPFC optimal placement [11]. The stability of a multi-machine system is determined with GUPFC device. The parameters of GUPFC are provided by flower pollination algorithm and controlled by two-stage lead-lag controller [12]. The on-load tap changer (OLTC) cannot be applicable for long radial feeders in distribution network toward voltage regulation. This problem is solved with a hybrid power compensation method D-GUPFC and is presented in [13]. The optimal reactive power dispatch (ORPD), the available transfer capacity, is enhanced by controlling the parameters of GUPFC using PSO algorithm [14]. The GUPFC optimal location is determined based on voltage variations to minimize total transmission loss and is presented in [15].

A similar device, PST, is the series-connected FACTS device used to control the power flow in the line. It consists of an exciting transformer, an injecting transformer and mechanical switches. The switches are used to change the turn's ratio of the transformer [16]. The combination of UPFC and a conventional PST is called as OUPFC which is the more cost-effective device in comparison with the standalone UPFC of same rating. An OPF with fuel cost and real power loss is formulated, and it is solved in MATLAB and General Algebraic Modeling System (GAMS) software environment by using OUPFC is proposed in [17]. A multi-objective function in terms of real power loss and voltage stability limit is solved by UPFC and OUPFC with firefly algorithm, and the superiority of OUPFC is observed [18]. The generation cost and transmission loss cost are reduced with OUPFC in [19] whose parameters are optimized by using genetic algorithm [20]. Voltage stability is improved in [21] under contingency conditions with OUPFC and HICA-PS algorithm. $(n-1)$ Line contingency analysis is performed to increase the

loadability with OUPFC device and is presented in [22]. The economic operation is performed in power systems to analyze the effect of OUPFC under weather changing conditions as well as variable loading conditions [23]. Transmission system security is enhanced under single line contingency conditions with OUPFC device under different renewable energy generations and is proposed in [24].

In light of the reviewed works, we claim that the following are the major contributions of this paper.

1. For the first time, a novel and advanced FACTS device, namely GOUPFC and its steady-state modeling, is introduced.
2. Besides, the optimal location and sizing of GOUPFC are determined using a novel hybrid approach WO-BAT.
3. In order to improve the exploitation features of WOA, a predefined search space for locations is defined using line collapse proximity indicator (LCPI) and its convergence features are improved using BAT algorithm.
4. The impact of GOUPFC is analyzed on IEEE 57-bus system considering line contingencies and renewable energy uncertainty.

Methods

It is possible to extend the voltage and power flow control beyond what can achievable with the OUPFC by using a new configuration is called as generalized optimal unified power flow controller (GOUPFC). To the best of our knowledge, no research work has been developed in the area of GOUPFC power injection modeling and its application to achieve the optimal operation of the power system. Firstly, the power injection modeling of GOUPFC device is presented by considering switching losses, and then, the optimal location is determined based on LCPI index. The control parameters of GOUPFC device are optimized with WO-BAT, WOA and BAT algorithms. Besides, the performance of GOUPFC is investigated under single line contingencies and with support of various renewable penetrations for standard IEEE-57 test system to minimize the objective function formulated in terms of AVDI, P_{loss} and $LCPI_{avg}$ and to enhance voltage profile.

This paper is organized in the following sections. Section 3 describes the operating principle of GOUPFC. Section 4 presents the mathematical modeling of GOUPFC. Section 5 presents the overall objective function formulation. Section 6 presents WO-BAT algorithm description, and Sect. 7 presents the determination of GOUPFC optimal location and the analytical results evaluated from different case studies.

Operating principle of GOUPFC

The transmission system security in the multi-lines can be enhanced by including another OUPFC in different line is not a cost-effective solution instead going for the new device named GOUPFC which is the best choice. The single line diagram of GOUPFC is shown in Fig. 1. It consists of one exciting transformer with four windings such as one primary winding and three secondary windings named as secondary, tertiary and quaternary and two triple winding injecting transformers each with one primary and two secondaries named as secondary and tertiary. The PST in one line is coupled to the two

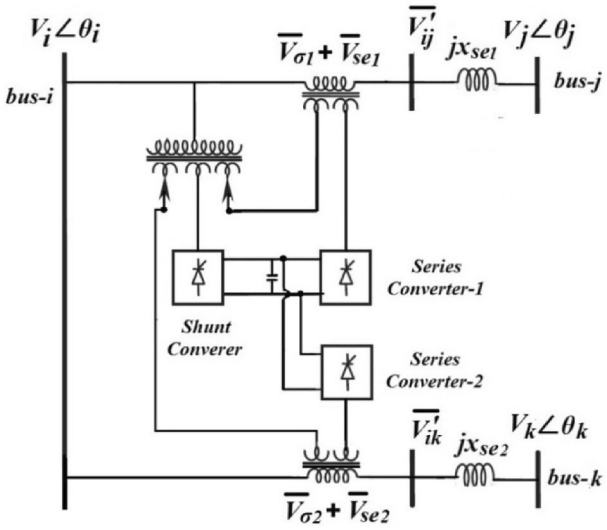

Fig. 1 Single line diagram of GOUPFC

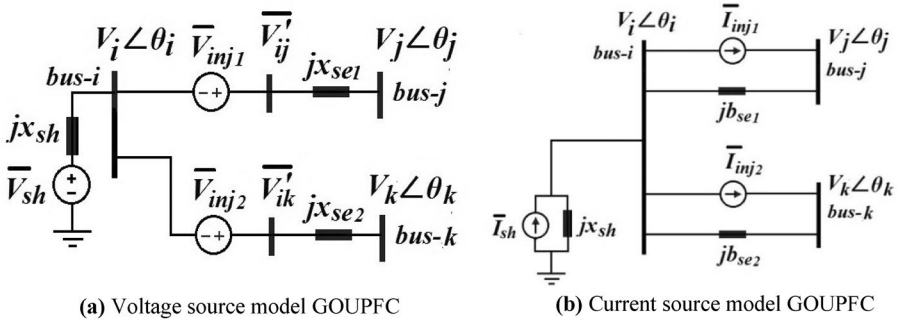

(a) Voltage source model GOUPFC **(b)** Current source model GOUPFC

Fig. 2 **a** Voltage source model GOUPFC, **b** current source model GOUPFC

secondary windings of the exciting and injecting transformers, and the PST in the other line is connected to the quaternary and secondary windings of the exciting and injecting transformer, respectively. One of the three converters is connected in shunt with a bus, and the remaining two converters are connected in series with two different transmission lines through the tertiary winding of the exciting and injecting transformers. The overall configuration of GOUPFC can able to control the total six control parameters which includes the controllable voltage magnitude and phase angles at bus-*i* and independent real and reactive power flows in the two lines. Figure 1 shows the two transmission lines *i*–*j* and *i*–*k* is connected with GOUPFC at buses *j* and *k*, respectively.

The series converter and PST will inject a controllable voltage magnitude and phase in series into the lines through injecting transformers. The shunt converter can able to (1) supply or absorb the real power needed by the series converter; (2) exchange the controllable reactive power with line; and (3) regulate the dc link voltage.

Mathematical modeling of GOUPFC

A GOUPFC can be represented by three controllable voltage source converters, and two-phase shifting transformers connected in two transmission lines is shown in Fig. 2.

The series converter controllable voltages and PST voltages are given by,

$$\left.\begin{array}{l} \overline{V_{\mathrm{se}_1}} = r_1 \overline{V_i} e^{j\gamma_1};\ \overline{V_{\mathrm{se}_2}} = r_2 \overline{V_i} e^{j\gamma_2} \\ \overline{V_{\sigma_1}} = k_1 \overline{V_i} e^{j\sigma_1};\ \overline{V_{\sigma_2}} = k_2 \overline{V_i} e^{j\sigma_2} \end{array}\right\} \tag{1}$$

where r_1, r_2 and k_1, k_2 are the per unit voltage magnitudes of two series converters and two PSTs, respectively;γ_1 and γ_2 are the phase angles of series converters; σ_1 and σ_2 are the PST phase angles; and V_i is the bus-i voltage. The voltages and phase angles are operating in the limits specified as follows.

$$\begin{array}{l} r_{\min} \le r \le r_{\max},\quad k_{\min} \le k \le k_{\max} \\ \gamma_{\min} \le \gamma \le \gamma_{\max},\ \sigma_{\min} \le \sigma \le \sigma_{\max} \end{array}$$

GOUPFC having three voltage source converters among those one is shunt converter, and the remaining two are series converters. Shunt converter is placed at bus-*I,* and the two series converters are placed in the lines *i–j* and *i–k*, respectively. In addition to the voltage source converters, GOUPFC employing two separate PSTs which are incorporated in the two separate lines where the two series converters are placed. The total voltages injected in the two lines are the phasor sum of the voltages obtained from the series converters and PSTs, and these are given by,

$$\overline{V_{\mathrm{inj}_1}} = \overline{V_{\mathrm{se}_1}} + \overline{V_{\sigma_1}};\quad \overline{V_{\mathrm{inj}_2}} = \overline{V_{\mathrm{se}_2}} + \overline{V_{\sigma_2}}$$

The GOUPFC is modeled in series-connected and shunt-connected voltage source models. The voltages in the two transmission lines behind the line reactance can be written mathematically as,

$$\overline{V'_{ij}} = \overline{V_{\mathrm{inj}_1}} + \overline{V_i};\quad \overline{V'_{ik}} = \overline{V_{\mathrm{inj}_2}} + \overline{V_i}$$

Series-connected voltage source model

The series-connected voltage source model of GOUPFC with three buses *i*, *j*, and *k* is shown in Fig. 2a, and the corresponding Norton's equivalent current source model is shown in Fig. 2b. Let the currents flowing in the two lines *i–j* and *i–k* are I_{se_1} and I_{se_2}, respectively, are given by

$$\left.\begin{array}{l} \overline{I_{\mathrm{se}_1}} = \dfrac{\overline{V_{\mathrm{inj}_1}}}{jX_{\mathrm{se}_1}} = -jB_{\mathrm{se}_1}\overline{V_{\mathrm{inj}_1}} = -B_{\mathrm{se}_1}V_i\left(r_1 e^{j(90+\gamma_1+\theta_i)} + k_1 e^{j(90+\sigma_1+\theta_i)}\right) \\ \overline{I_{\mathrm{se}_2}} = \dfrac{\overline{V_{\mathrm{inj}_2}}}{jX_{\mathrm{se}_2}} = -jB_{\mathrm{se}_2}\overline{V_{\mathrm{inj}_2}} = -B_{\mathrm{se}_2}V_i\left(r_2 e^{j(90+\gamma_2+\theta_i)} + k_2 e^{j(90+\sigma_2+\theta_i)}\right) \end{array}\right\} \tag{2}$$

where X_{se_1} and X_{se_2} are the line reactances of the two lines and their corresponding susceptances, respectively, given by, $B_{\mathrm{se}_1} = 1/X_{\mathrm{se}_1}$ and $B_{\mathrm{se}_2} = 1/X_{\mathrm{se}_2}$.

The independent complex power injections of GOUPFC at buses *i*, *j* and *k* are given as,

$$\overline{S_{i\mathrm{se}}} = -\overline{V_i}\left(\overline{I_{\mathrm{se}_1}}\right)^* - \overline{V_i}\left(\overline{I_{\mathrm{se}_1}}\right)^*$$

$$\overline{S_{i\mathrm{se}}} = -V_i^2 B_{\mathrm{se}_1}\left(r_1 e^{-j(90+\gamma_1)} + k_1 e^{-j(90+\sigma_1)}\right) - V_i^2 B_{\mathrm{se}_2}\left(r_2 e^{-j(90+\gamma_2)} + k_2 e^{-j(90+\sigma_2)}\right) \tag{3}$$

$$\overline{S_{jse}} = \overline{V_j}\left(\overline{I_{se_1}}\right)^* = -V_i V_j B_{se_1}\left(r_1 e^{-j(90+\gamma_1+\theta_i-\theta_j)} + k_1 e^{-j(90+\sigma_1+\theta_i-\theta_j)}\right) \tag{4}$$

$$\overline{S_{kse}} = \overline{V_k}\left(\overline{I_{se_2}}\right)^* = -V_i V_k B_{se_2}\left(r_2 e^{-j(90+\gamma_2+\theta_i-\theta_k)} + k_2 e^{-j(90+\sigma_2+\theta_i-\theta_k)}\right) \tag{5}$$

Let $\theta_{ij} = \theta_i - \theta_j$; $\theta_{ik} = \theta_i - \theta_k$. By using Euler's and trigonometric identities, the real and reactive power injections at the buses *i*, *j* and *k* are calculated as follows.

$$P_{i_{se}} = -V_i^2 B_{se_1}(r_1 \sin(\gamma_1) + k_1 \sin(\sigma_1)) - V_i^2 B_{se_2}(r_2 \sin(\gamma_2) + k_2 \sin(\sigma_2)) \tag{6}$$

$$Q_{i_{se}} = -V_i^2 B_{se_1}(r_1 \cos(\gamma_1) + k_1 \cos(\sigma_1)) - V_i^2 B_{se_2}(r_2 \cos(\gamma_2) + k_2 \cos(\sigma_2)) \tag{7}$$

$$P_{j_{se}} = V_i V_j B_{se_1}(r_1 \sin(\gamma_1 + \theta_{ij}) + k_1 \sin(\sigma_1 + \theta_{ij})) \tag{8}$$

$$Q_{j_{se}} = V_i V_j B_{se_1}(r_1 \cos(\gamma_1 + \theta_{ij}) + k_1 \cos(\sigma_1 + \theta_{ij})) \tag{9}$$

$$P_{k_{se}} = V_i V_k B_{se_2}(r_2 \sin(\gamma_2 + \theta_{ik}) + k_2 \sin(\sigma_2 + \theta_{ik})) \tag{10}$$

$$Q_{k_{se}} = V_i V_k B_{se_2}(r_2 \cos(\gamma_2 + \theta_{ik}) + k_2 \cos(\sigma_2 + \theta_{ik})) \tag{11}$$

The equivalent power injection modeling for the series-connected voltage source model is shown in Fig. 3a. The amount of complex power supplied by the combination of series converter and PST in the individual lines is derived as follows

$$\begin{aligned} \overline{S_{se_1}} &= P_{se_1} + jQ_{se_1} = \overline{V_{inj_1}}\left(\overline{I_{ij}}\right)^* \\ \overline{S_{se_1}} &= jB_{se_1} V_i\left(r_1 e^{j(\gamma_1+\theta_i)} + k_1 e^{j(\sigma_1+\theta_i)}\right)\left(\overline{V'_{ij}} - \overline{V_j}\right)^* \end{aligned} \tag{12}$$

$$\begin{aligned} \overline{S_{se_2}} &= P_{se_2} + jQ_{se_2} = \overline{V_{inj_2}}\left(\overline{I_{ik}}\right)^* \\ \overline{S_{se_2}} &= jB_{se_2} V_i\left(r_2 e^{j(\gamma_2+\theta_i)} + k_2 e^{j(\sigma_2+\theta_i)}\right)\left(\overline{V'_{ik}} - \overline{V_k}\right)^* \end{aligned} \tag{13}$$

The real and reactive powers supplied by the two converters in the two transmission lines are given by,

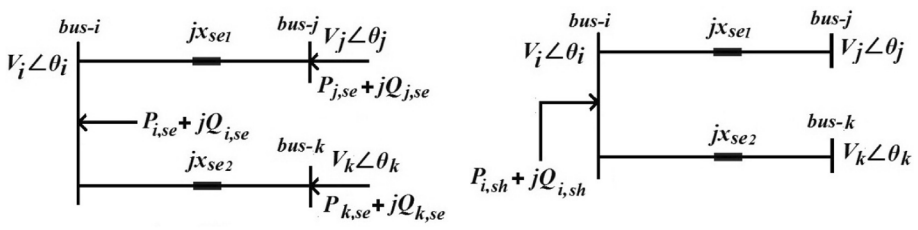

(a) Equivalent series connected model **(b)** Equivalent shunt connected model

Fig. 3 **a** Equivalent series connected model, **b** equivalent shunt connected model

$$\begin{aligned} P_{\mathrm{se}_1} = & -r_1 B_{\mathrm{se}_1} V_i^2 \sin(\gamma_1) - k_1 B_{\mathrm{se}_1} V_i^2 \sin(\sigma_1) \\ & + r_1 B_{\mathrm{se}_1} V_i V_j \sin\left(\gamma_1 + \theta_{ij}\right) + k_1 B_{\mathrm{se}_1} V_i V_j \sin\left(\sigma_1 + \theta_{ij}\right) \end{aligned} \tag{14}$$

$$\begin{aligned} Q_{\mathrm{se}_1} = & B_{\mathrm{se}_1} V_i^2 \left(r_1^2 + k_1^2\right) + 2 r_1 k_1 B_{\mathrm{se}_1} V_i^2 \cos(\sigma_1 - \gamma_1) \\ & + r_1 B_{\mathrm{se}_1} V_i^2 \cos(\gamma_1) + k_1 B_{\mathrm{se}_1} V_i^2 \cos(\sigma_1) \\ & - r_1 B_{\mathrm{se}_1} V_i V_j \cos\left(\gamma_1 + \theta_{ij}\right) - k_1 B_{\mathrm{se}_1} V_i V_j \cos\left(\sigma_1 + \theta_{ij}\right) \end{aligned} \tag{15}$$

$$\begin{aligned} P_{\mathrm{se}_2} = & -r_2 B_{\mathrm{se}_2} V_i^2 \sin(\gamma_2) - k_2 B_{\mathrm{se}_2} V_i^2 \sin(\sigma_2) \\ & + r_2 B_{\mathrm{se}_2} V_i V_k sin(\gamma_2 + \theta_{ik}) + k_2 B_{\mathrm{se}_2} V_i V_k sin(\sigma_2 + \theta_{ik}) \end{aligned} \tag{16}$$

$$\begin{aligned} Q_{\mathrm{se}_2} = & B_{\mathrm{se}_2} V_i^2 \left(r_2^2 + k_2^2\right) + 2 r_2 k_2 B_{\mathrm{se}_2} V_i^2 \cos(\sigma_2 - \gamma_2) \\ & + r_2 B_{\mathrm{se}_2} V_i^2 \cos(\gamma_2) + k_1 B_{\mathrm{se}_1} V_i^2 \cos(\sigma_2) \\ & - r_2 B_{\mathrm{se}_2} V_i V_k \cos(\gamma_2 + \theta_{ik}) - k_2 B_{\mathrm{se}_2} V_i V_k \cos(\sigma_2 + \theta_{ik}) \end{aligned} \tag{17}$$

Shunt-connected voltage source model

The equivalent circuit for the shunt-connected voltage source model is shown in Fig. 3b. This model provides the equivalent power injections at the GOUPFC shunt bus to the two series branches through the converter and PST combination. The voltage at the sending end is controlled by the reactive power injection at the GOUPFC shunt converter. The amount of real power supplied by the shunt converter is equal to the real power consumed by the two series converters. Therefore, the real power inserted at the shunt converter is given by:

$$P_{\mathrm{sh}} = -\left(P_{\mathrm{se}_1} + P_{\mathrm{se}_2}\right)$$

$$\begin{aligned} P_{\mathrm{sh}} = & r_1 B_{\mathrm{se}_1} V_i^2 \sin(\gamma_1) + k_1 B_{\mathrm{se}_1} V_i^2 \sin(\sigma_1) + r_2 B_{\mathrm{se}_2} V_i^2 \sin(\gamma_2) + k_2 B_{\mathrm{se}_2} V_i^2 \sin(\sigma_2) \\ & - r_1 B_{\mathrm{se}_1} V_i V_j \sin\left(\gamma_1 + \theta_{ij}\right) - k_1 B_{\mathrm{se}_1} V_i V_j \sin\left(\sigma_1 + \theta_{ij}\right) \\ & - r_2 B_{\mathrm{se}_2} V_i V_k \sin(\gamma_2 + \theta_{ik}) - k_2 B_{\mathrm{se}_2} V_i V_k \sin(\sigma_2 + \theta_{ik}) \end{aligned} \tag{18}$$

Let assume a constant reactive power injection Q_{sh} at bus-i and the apparent power injection at the shunt bus-i is given as

$$S_{\mathrm{sh}} = P_{\mathrm{sh}} + jQ_{\mathrm{sh}}$$

Final GOUPFC modeling

The final PIM of GOUPFC is achieved by summing up the equations obtained in series- and shunt-connected models. The corresponding equivalent circuit representing GOUPFC power injection is shown in Fig. 4. The resultant real and reactive power equations at the GOUPFC buses are given as

$$P_{i_{\mathrm{goupfc}}} = P_{i_{\mathrm{se}}} + P_{\mathrm{sh}}$$

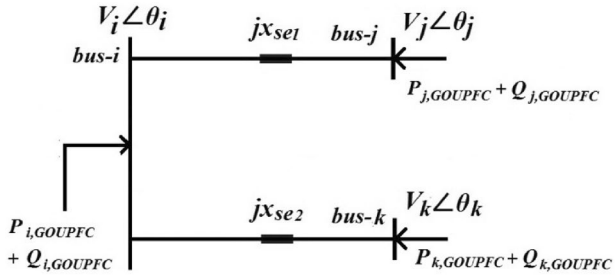

Fig. 4 Final GOUPFC mathematical model

$$\begin{aligned} P_{i_{\text{goupfc}}} = & -r_1 B_{\text{se}_1} V_i V_j \sin\left(\gamma_1 + \theta_{ij}\right) - k_1 B_{\text{se}_1} V_i V_j \sin\left(\sigma_1 + \theta_{ij}\right) \\ & - r_2 B_{\text{se}_2} V_i V_k \sin\left(\gamma_2 + \theta_{ik}\right) - k_2 B_{\text{se}_2} V_i V_k \sin\left(\sigma_2 + \theta_{ik}\right) \end{aligned} \tag{19}$$

$$Q_{i_{\text{goupfc}}} = Q_{i_{\text{se}}} + Q_{\text{sh}}$$

$$\begin{aligned} Q_{i_{\text{goupfc}}} = & -V_i^2 B_{\text{se}_1}\left(r_1 \cos\left(\gamma_1\right) + k_1 \cos\left(\sigma_1\right)\right) \\ & - V_i^2 B_{\text{se}_2}\left(r_2 \cos\left(\gamma_2\right) + k_2 \cos\left(\sigma_2\right)\right) + Q_{\text{sh}} \end{aligned} \tag{20}$$

$$P_{j_{\text{goupfc}}} = P_{j_{\text{se}}} = V_i V_j B_{\text{se}_1}\left(r_1 \sin\left(\gamma_1 + \theta_{ij}\right) + k_1 \sin\left(\sigma_1 + \theta_{ij}\right)\right) \tag{21}$$

$$Q_{j_{\text{goupfc}}} = Q_{j_{\text{se}}} = V_i V_j B_{\text{se}_1}\left(r_1 \cos\left(\gamma_1 + \theta_{ij}\right) + k_1 \cos\left(\sigma_1 + \theta_{ij}\right)\right) \tag{22}$$

$$P_{k_{\text{goupfc}}} = P_{k_{\text{se}}} = V_i V_k B_{\text{se}_2}\left(r_2 \sin\left(\gamma_2 + \theta_{ik}\right) + k_2 \sin\left(\sigma_2 + \theta_{ik}\right)\right) \tag{23}$$

$$Q_{k_{\text{goupfc}}} = Q_{k_{\text{se}}} = V_i V_k B_{\text{se}_2}\left(r_2 \cos\left(\gamma_2 + \theta_{ik}\right) + k_2 \cos\left(\sigma_2 + \theta_{ik}\right)\right) \tag{24}$$

Overall objective function (OOF) formulation

An OPF-based multi-objective function is formulated to minimize the overall objective function (OOF) is given as,

$$\text{OOF} = w_1 f_1 + w_2 f_2 + w_3 f_3 \tag{25}$$

where w_1, w_2 and w_3 are the weighing factors considered as one. f_1, f_2 and f_3 are the AVDI, P_{loss} and average LCPI, respectively.

Average voltage deviation index (AVDI)

The voltage profile of the test system subjected to contingency condition is evaluated in terms of stability index called AVDI. It is given as [23],

$$f_1 = \text{AVDI} = \frac{1}{\text{nb}} \sum_{i=1}^{\text{nb}} \left(\frac{|V_{i,\text{ref}}| - |V_i|}{|V_{i,\text{ref}}|} \right)^2$$

where $|V_{i,\text{ref}}|$ is the reference voltage at bus-i, $|V_i|$ is the voltage at bus-i under contingencies and nb is the number of load buses.

In specific, AVDI is used to explain the average voltage deviation of the entire network in comparison with the reference bus voltage (i.e., maximum of all bus voltages). Under each contingency, the voltage profile may change, and thus, there is a change in AVDI. The more AVDI means, more voltage imbalance in the network.

Real power loss (P_{loss})

The real power loss is given mathematically as,

$$f_2 = P_{\text{loss}} = \sum_{k=1}^{\text{nl}} I_k^2 r_k$$

$$f_2 = \sum_{i=1}^{\text{nb}} \sum_{\substack{j=1 \\ j \neq i}}^{\text{nb}} \left\{ Y_{ii} \cos \theta_{ii} \left[V_i^2 + V_j^2 - 2V_i V_j \cos\left(\delta_i - \delta_j\right) \right] \right\}$$

where nb is no. of buses; nl is no. of lines; k is the line number; r_k and I_k are the resistance of line k and current through it, respectively; Y_{ii} and θ_{ij} are the shunt admittance at bus i and its angle, respectively; V_i and δ_i are the voltage magnitude and its angle at bus-i, respectively; V_j and δ_j are the voltage and its angle at bus$j$, respectively.

Line collapse proximity index (LCPI)

The error in evaluating the voltage stability due to neglecting the line charging reactance and the magnitude and relative directions of active and reactive power can be overcome by considering an index called LCPI [25]. LCPI is given as,

$$f_3 = \text{LCPI} = \frac{4A \cos(\alpha)\left(P_j B \cos(\beta) + Q_j B \sin(\beta)\right)}{\left(V_i \cos(\delta)\right)^2}$$

where A and B are network parameters magnitude; α and β are the phases of A and B, respectively; and V_i is the sending end voltage.P_j and Q_j are the real and reactive power flow; for a line, LCPI should always less than 1 failing leads to instability.

Constraints

The OOF expressed in Eq. (25) is subjected to various equality and inequality constraints [21] as given below.

Equality constraints

The active and reactive power balance equations are the equality constraints that can be expressed, for all the buses expect FACTS incident buses, as

$$P_i = P_{gi} - P_{di(t)} = \sum_{k=1}^{\text{nb}} |V_i||V_k||Y_{ik}| \cos(\theta_{ik} - \delta_i + \delta_k), \quad \forall i \in 1, 2, \ldots, \text{nb} \tag{26}$$

$$Q_i = Q_{gi} - Q_{di(t)} = \sum_{k=1}^{\text{nb}} |V_i||V_k||Y_{ik}| \sin(\theta_{ik} - \delta_i + \delta_k), \quad \forall i \in 1, 2, \ldots, \text{nb} \tag{27}$$

The active and reactive power balance equations at the FACTS incident buses are given as,

$$\begin{aligned} &P_i = P_{gi} - (P_{di(t)} + P_{\text{inj},i}); \quad \forall i \in 1, 2, \ldots, \text{nb} \\ &P_i = \sum_{k=1}^{\text{nb}} |V_i||V_k||Y_{ik}| \cos(\theta_{ik} - \delta_i + \delta_k) \end{aligned} \tag{28}$$

$$\begin{aligned} &Q_i = Q_{gi} - (Q_{di(t)} + Q_{\text{inj},i}); \quad \forall i \in 1, 2, \ldots, \text{nb} \\ &Q_i = -\sum_{k=1}^{\text{nb}} |V_i||V_k||Y_{ik}| \sin(\theta_{ik} - \delta_i + \delta_k) \end{aligned} \tag{29}$$

Inequality constraints

The inequality constraints considered for optimization problem are given as follows.

$$P_{gi,r}^{\min} \le P_{gi,r} \le P_{gi,r}^{\max} \quad \forall i \in \text{ng}, \tag{30}$$

$$Q_{gi,r}^{\min} \le Q_{cg,i} \le Q_{gi,r}^{\max} \quad \forall i \in \text{ng}, \tag{31}$$

$$|V_i^{\min}| \le |V_i| \le |V_i^{\max}| \quad \forall i \in \text{nb}, \tag{32}$$

$$\delta_i^{\min} \le \delta_i \le \delta_i^{\max} \quad \forall i \in \text{nb}, \tag{33}$$

$$a_i^{\min} \le a_i \le a_i^{\max} \quad \forall i = \text{ntcl}, \tag{34}$$

$$Q_{c,\text{inj},i}^{\min} \le Q_{c,\text{inj},i} \le Q_{c,\text{inj},i}^{\max} \quad \forall i = \text{nvcb}, \tag{35}$$

$$\left|S_l| \le |S_l^{\max}\right| \quad \forall l = \text{nl}, \tag{36}$$

WO-BAT algorithm

In this paper, the control parameters of GOUPFC device are optimized with the hybrid algorithm WO-BAT. The detailed description about WO-BAT is described as follows.

Whale optimization algorithm

The exploitation and exploration are the two stages involved in WOA [26]. In exploitation stage, surrounding prey and spiral updation of the position vector are modeled. This method is called bubble net attacking (BNA) method [27]. Random searching of prey is performed in exploitation stage. After identifying the position of prey, humpback whales surround them. Initially, the optimal location of prey in the search space is not defined. Therefore, this algorithm considers the present solution which is the optimal prey and the other search delegates (agents) will drifted toward the best search delegates. This can be expressed mathematically as,

$$\overrightarrow{P}(t+1) = \overrightarrow{P^*}(t) - \overrightarrow{C_1} \cdot \overrightarrow{D} \tag{37}$$

$$\overrightarrow{D} = \left| \overrightarrow{C_2} \cdot \overrightarrow{P^*}(t) - \overrightarrow{P}(t) \right| \tag{38}$$

where $\overrightarrow{P^*}(t)$ is the best location of whale at tth iteration; $\overrightarrow{P}(t+1)$ is the present position of whale; $\overrightarrow{D}$ is a vector indicates the distance between whale and prey; the coefficient vectors $\overrightarrow{C_1}$ and $\overrightarrow{C_2}$ are calculated as follows,

$$\overrightarrow{C_1} = 2 \cdot \overrightarrow{i} \cdot \overrightarrow{r} + \overrightarrow{i}; \quad \overrightarrow{C_2} = 2 \cdot \overrightarrow{r} \tag{39}$$

The range of vector $\overrightarrow{C_1}$ is $(-i, i)$ where i value is shrinking from 2 to 0 through iterations. The new position of search delegate is determined by choosing the random value for $\overrightarrow{C_1}$ in the interval $(-1, 1)$.

Consider whale and prey are located at (P, Q) and (P^*, Q^*). The equation for position between whale and prey gives a helix-shaped movement of whale, and it is given as:

$$\overrightarrow{P}(t+1) = e^{ck} \cdot \cos(2\pi k) \cdot \overrightarrow{D^*} + \overrightarrow{P^*}(t); \tag{40}$$

$$\overrightarrow{D^*} = \left| \overrightarrow{P^*}(t) - \overrightarrow{P}(t) \right| \tag{41}$$

where c is a constant which recognize the logarithmic spiral shape and k is a random number in the range $[-1, 1]$.

Therefore, the final position vector equation w.r.t. a reference number n (0, 1) is represented as,

$$\overrightarrow{P}(t+1) = \begin{cases} \overrightarrow{P^*}(t) - \overrightarrow{C_1} \cdot \overrightarrow{D}, & \text{if } n < 0.5 \\ e^{ck} \cdot \cos(2\pi k) \cdot \overrightarrow{D^*} + \overrightarrow{P^*}(t), & \text{if } n \geq 0.5 \end{cases} \tag{42}$$

In the exploration stage, to compel the search delegates to move far away from the local whale, the coefficient vector $\overrightarrow{C_1}$ is used to generate random values less or greater than one. The location of delegates is identified based on this random selection rather than the best search delegate. This gives the global solution by overcoming the location solution. This can be given mathematically,

$$\overrightarrow{P}(t+1) = \overrightarrow{P_{\text{rand}}} - \overrightarrow{C_1} \cdot \overrightarrow{D} \tag{43}$$

$$\overrightarrow{D} = \left| \overrightarrow{C_2} \cdot \overrightarrow{P_{\text{rand}}} - \overrightarrow{P} \right| \tag{44}$$

where $\overrightarrow{P_{\text{rand}}}$ is the random position vector.

Bat algorithm

Bats are the creatures with echo-location abilities. They create a loud sound pulse and receive the echo from the neighboring objects. They can guess the position of the neighboring object by using the time delay of echo sound. They measure the shape and the direction of object by sound pulse comparative amplitude analysis received at the ear. They investigate and simplify the data collected and figured out an image in brain to identify the neighboring object. The concept of bat algorithm (BA) and its mathematical modeling is provided in [28].

To determine the location of prey, bats fly randomly in the search space with a velocity v_{i}. Later, they change their positions (x_{i}) with constant frequency (f_{min}), different wavelengths (β) and loudness A_0. The new solutions for position and velocity are given mathematically as,

$$f_i = f_{\text{min}} + (f_{\text{max}} - f_{\text{min}}) \cdot \beta, \tag{45}$$

$$v_i^t = v_i^{t-1} + (x_i^t - x_*) \cdot f_i, \tag{46}$$

$$x_i^t = x_i^{t-1} + v_i^t, \tag{47}$$

where β is a random number obtained by uniform distribution in the range [0, 1]. x^* is the present global best; the minimum and maximum frequency limits (f_{min} and f_{max}) are taken 0 and 100, respectively.

WO-BAT algorithm

The major limitation of WOA is its convergence speed in obtaining global solution. However, this can be overcome by embedding BAT algorithm partially to WOA to increase the exploration. In this hybrid algorithm, the global position is updated based on condition technique, which means if the present solution is better than the old solution, then the old one can be replaced with the present solution. The detailed flowchart for this hybrid algorithm is shown in Fig. 5.

Results and discussions

The performance of GOUPFC device is analyzed under single line contingencies, and an OPF-based objective function is solved by using WO-BAT, WOA and BAT algorithms under the different RES penetrations. The test system data are taken from [29]. In comparison with earlier works [23, 24], this work is focused on the development of mathematical modeling for the novel GOUPFC and its location and parameters

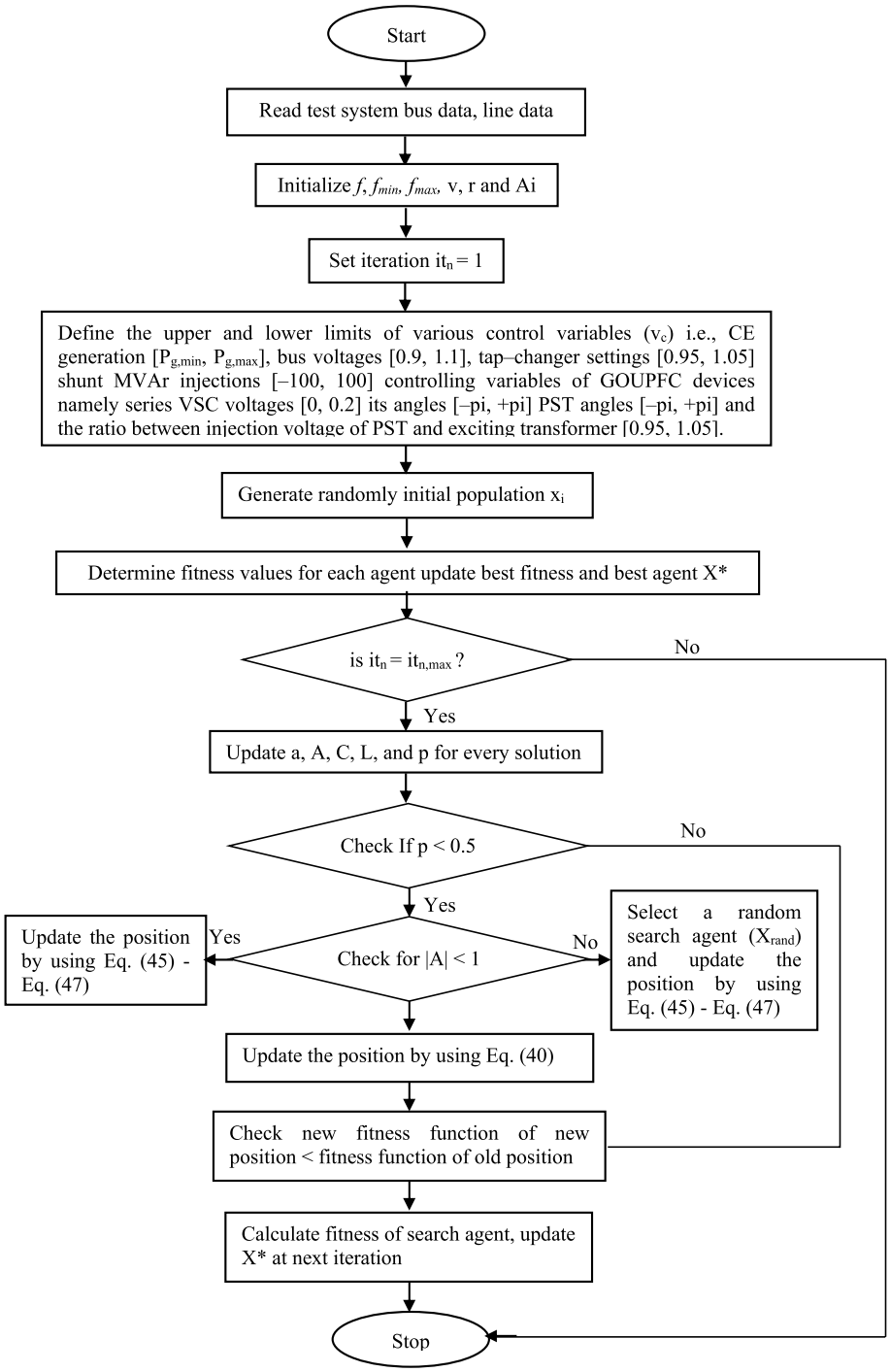

Fig. 5 Flow chart of proposed methodology using WO-BAT

optimization using novel hybrid approach WO-BAT in this work. The type of RES considered in this work is photovoltaic system, and its mathematical modeling is adapted from Ref. [23]. The simulations are carries under five different cases:

Table 1 Optimal location of GOUPFC based on LCPI

S. No.	Line No	From bus	To bus	LCPI
1	**78**	**38**	**49**	**0.10385**
2	70	54	55	0.08561
3	43	30	31	0.08302
4	**50**	**37**	**38**	**0.07946**
5	69	53	54	0.07176

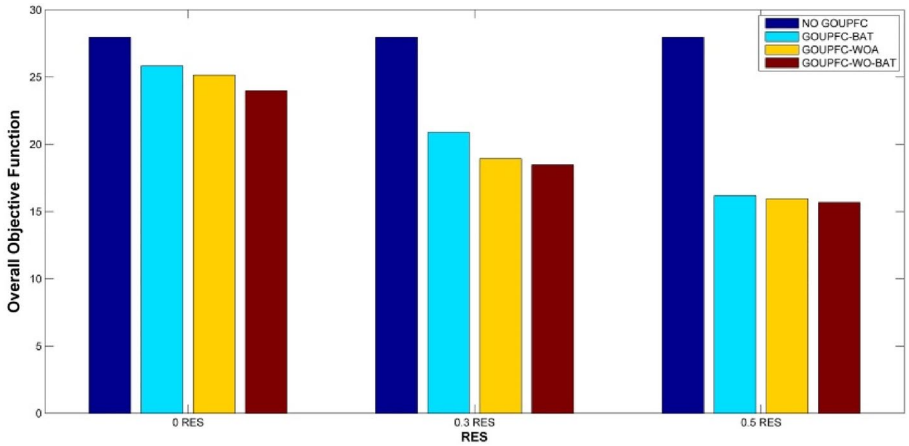

Fig. 6 GOUPFC under without contingency and at different RES penetration levels

Case 1: Performance of GOUPFC under one line contingency condition and with the support of RES penetrations.
Case 2: One line contingency without GOUPFC as well as RES penetrations.
Case 3: One line contingency only with GOUPFC.
Case 4: One line contingency with GOUPFC and 30% RES penetrations.
Case 5: One line contingency with GOUPFC and 50% RES penetrations.

Optimal location of GOUPFC

Under base case conditions (i.e., no GOUPFC device and no RES), LCPI is calculated for all the lines of IEEE-57 test system and arranged in descending order as shown in Table 1. The top 5 ranked locations are only shown here after excluding the lines incident to generator and tap setting transformer. From Table 1, the two lines 38–49 (#78) and 37–38 (#50) are chosen for the placement of GOUPFC device. The shunt converter is placed at the bus#38 which is the common bus to the two line and the two series converters are placed in the two lines.

IEEE-57 bus description

IEEE-57 bus test system has 7 PV buses (i.e., 1, 2, 3, 6, 8, 9 and 12) and 50 PQ buses interconnected by 80 transmission lines. It has real and reactive power loads, respectively,

1250.8 MW and 336.4 MVAr. To maintain the continuity of supply, the lines 32–33 (#45) and 35–36 (#48) are not considered for contingency analysis. By excluding these two lines from 80 lines, the contingency analysis is performed on the remaining 78 lines and the results are demonstrated here.

In case 1, the GOUPFC is tested under normal conditions considering different RES penetrations. The device parameters are optimized with the three algorithms, and the objective function values are shown in Fig. 6. From this figure, under no contingency conditions, GOUPFC along with 50% RES penetration level gives minimum OOF value for WO-BAT algorithm. In other words, as RES penetration increases the net effective loading on the system decreases. Thus, the OOF is decreased. However, by having GOPUF controls, it is further decreases. The optimal controls derived with WO-BAT are caused to improve the system performance than basic WOA and BAT, significantly.

In case2, the system is suffering with single line contingency and there is no support from GOUPFC device and RES generation. Under these conditions, the performance indices and OOF for no contingency and one line contingency are presented in Table 2. The system has real power loss and LCPI value with no contingency 27.8638 MW and 0.081, respectively, and the objective function value 27.9448. A contingency analysis is performed on the system without GOUPFC and RES, and the indices for the top ranked line 54–55 (#70) are as follows: $P_{\text{loss}} = 29.7828$, ALCPI = 0.0860 and OOF = 29.8688. The individual objective functions and OOF values for the remaining lines are presented in Table 2.

In case 3, the integration of GOUPFC without RES is analysed under one line contingencies. The parameters of the GOUPFC device are optimized WO-BAT, WOA and BAT algorithms, and the results are demonstrated in Table 3. When there is no outage the real power loss is decreased to 22.9129 MW which is 17.77% decrement with reference to case 1. Under single line 54–55 (#70) contingency also GOUPFC has shown its superiority in terms of losses and LCPI value. The indices in one line contingency are $P_{\text{loss}} = 25.1792$, ALSI = 0.0467, ALCPI = 0.0747 and OOF = 25.2539. Here, the real power loss and OOF have been reduced to 34.18% and 51.83%, respectively, with reference to case 1. The LCPI and OOF values for other lines are presented in Table 3. The

Table 2 Single line contingency without GOUPFC and RES

Line contingency	AVDI	P_{loss} (MW)	LCPI_{avg}	OOF
–	0.0122	27.8638	0.0810	27.957
54–55	0.0169	31.6620	0.0936	31.773
30–31	0.0135	29.7828	0.0860	29.882
37–38	0.0140	28.5135	0.0853	28.613
53–54	0.0125	27.7525	0.0825	27.848
50–51	0.0134	28.1352	0.0846	28.233
46–47	0.0155	30.1610	0.0878	30.264
41–42	0.0124	27.9146	0.0820	28.009
18–19	0.0127	28.6013	0.0837	28.698
25–30	0.0129	28.1856	0.0816	28.280
38–48	0.0238	31.3219	0.1093	31.455

Table 3 GOUPFC under single line contingency conditions without RES

Line contingency	AVD			PLOSS			$LCPI_{avg}$			OOF		
	BAT	WOA	WO-BAT	BAT	WOA	WO-BAT	BAT	WOA	WO-BAT	BAT	WOA	WO-BAT
–	0.0095	0.0080	0.0037	25.7411	24.0541	22.9129	0.0795	0.0774	0.0656	25.8301	24.1395	22.9822
38–49	0.0091	0.0083	0.0056	25.7131	25.5613	24.8907	0.0783	0.0718	0.0699	25.8005	25.6414	24.9662
54–55	0.0124	0.0094	0.0051	26.6459	25.6800	25.1792	0.0867	0.0761	0.0747	26.745	25.7655	25.259
30–31	0.0112	0.0101	0.0073	25.8862	25.8124	25.4048	0.0790	0.0767	0.0736	25.9764	25.8992	25.4857
37–38	0.0265	0.0218	0.0200	29.8423	28.8470	28.2986	0.1097	0.1042	0.0997	29.9785	28.973	28.4183
53–54	0.0092	0.0087	0.0070	26.1754	25.9726	25.9248	0.0748	0.0743	0.0722	26.2594	26.0556	26.004
50–51	0.0093	0.0084	0.0077	25.6284	25.5713	25.2467	0.0770	0.0750	0.0688	25.7147	25.6547	25.3232
46–47	0.0111	0.0097	0.0064	28.0277	26.8253	26.1605	0.0837	0.0812	0.0714	28.1225	26.9162	26.2383
41–42	0.0112	0.0059	0.0059	26.6106	26.2942	25.3860	0.0870	0.0741	0.0690	26.7088	26.3742	25.4609
18–19	0.0128	0.0106	0.0081	25.9255	24.9389	24.8706	0.0776	0.0776	0.0774	26.0159	25.0271	24.9561
25–30	0.0114	0.0101	0.0046	29.0998	28.3871	27.1199	0.0762	0.0747	0.0629	29.1874	28.4719	27.1874

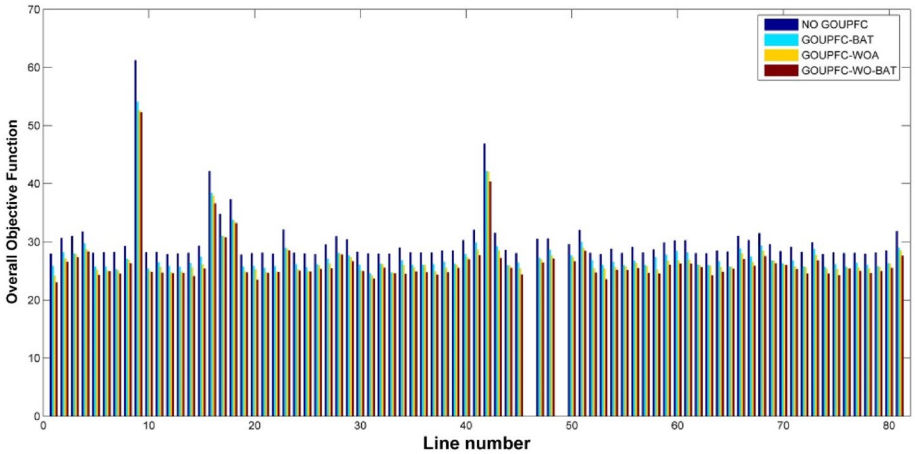

Fig. 7 GOUPFC performance under single contingency without RES

performance of GOUPFC under one line contingency at without RES for three algorithms is shown in Fig. 7.

In case 4, GOUPFC and 30% power penetration are together considered for the contingency. Here, the RES installed capacity is 30% of the real power load, i.e., $1250.8 \times 0.3 = 375.24$ MW. Therefore, the remaining load on the CE sources is 875.56 MW. Due to the integration of GOUPFC and RES into the system, the line flows and hence transmission losses are reduced under without and with line contingency conditions. The performance indices are evaluated for the both the conditions, and the losses are reduced by 37.57% and 34.18%, respectively. The optimized OOF values by WO-BAT algorithm are 17.4563 and 19.6639, respectively, for without and with line (54–55) contingency conditions. The individual objective functions and OOF for the remaining line contingencies are presented in Table 4. The performance of GOUPFC under single line contingency with0.3penetrations is shown in Fig. 8.

In case 5, the RES generation is enhanced to 50% and the support of GOUPFC device is still present. Here the RES installed capacity is 50% of the real power load, i.e., $1250.8 \times 0.5 = 625.4$ MW. Hence the remaining load on the CE sources is to be 625.4 MW. The control variables of GOUPFC device are optimized with three algorithms, and the results of WO-BAT are demonstrated here due to its superiority. Under no contingency condition, the performance indices with WO-BAT algorithm are $P_{\text{loss}} = 14.1166$, ALCPI = 0.0566 and the OOF = 14.2489. Here, the power loss and OOF are diminished by 49.34% and 96.90%, respectively, with respect to case 1. Under contingency conditions, the line 54–55 (#70) with performance indices as $P_{\text{loss}} = 15.2089$, ALCPI = 0.0506 and the OOF = 15.3261. Here also the combination of GOUPFC and 50% RES penetration level reduces the real power losses and OOF by 48.93% and 95.64%, respectively, with respect to case 1. The P_{loss}, LCPI_{avg} values and the corresponding OOF for the remaining line outages are presented in Table 5. The performance of GOUPFC under single line contingency with0.5penetrationsis shown in Fig. 9.

Table 4 GOUPFC under single line contingency and 0.3 RES

Line contingency	AVD			PLOSS			$LCPI_{avg}$			OOF		
	BAT	WOA	WO-BAT	BAT	WOA	WO-BAT	BAT	WOA	WO-BAT	BAT	WOA	WO-BAT
–	0.0075	0.0048	0.0028	20.8213	15.170	17.3955	0.0630	0.0608	0.0579	20.8918	18.9278	17.4562
38–49	0.0089	0.0079	0.0072	20.5125	14.410	18.0192	0.0730	0.0626	0.0583	20.5944	19.2026	18.0847
54–55	0.0099	0.0057	0.0049	20.8914	14.741	19.6030	0.0629	0.0614	0.0609	20.9642	20.4793	19.6688
30–31	0.0110	0.0081	0.0056	20.3284	14.540	18.2443	0.0755	0.0697	0.0639	20.4149	19.8867	18.3138
37–38	0.0155	0.0118	0.0105	20.7261	14.112	18.7019	0.0896	0.0822	0.0789	20.8312	20.0659	18.7913
53–54	0.0056	0.0052	0.0043	21.2083	14.404	19.7277	0.0674	0.0602	0.0587	21.2813	20.5989	19.7907
50–51	0.0112	0.0063	0.0047	20.5972	14.707	16.3334	0.0723	0.0608	0.0595	20.6807	18.2805	16.3976
46–47	0.0072	0.0047	0.0046	20.1629	14.750	19.3329	0.0656	0.0636	0.0546	20.2357	19.7054	19.3921
41–42	0.0108	0.0101	0.0076	20.4827	14.829	19.2511	0.0763	0.0757	0.0656	20.5698	19.7114	19.3243
18–19	0.0121	0.0082	0.0034	20.5838	19.737	19.0443	0.0659	0.0655	0.0653	20.6618	19.8028	19.113
25–30	0.0122	0.0119	0.0081	20.9185	14.646	19.4162	0.0838	0.0760	0.0698	21.0145	20.1884	19.4941

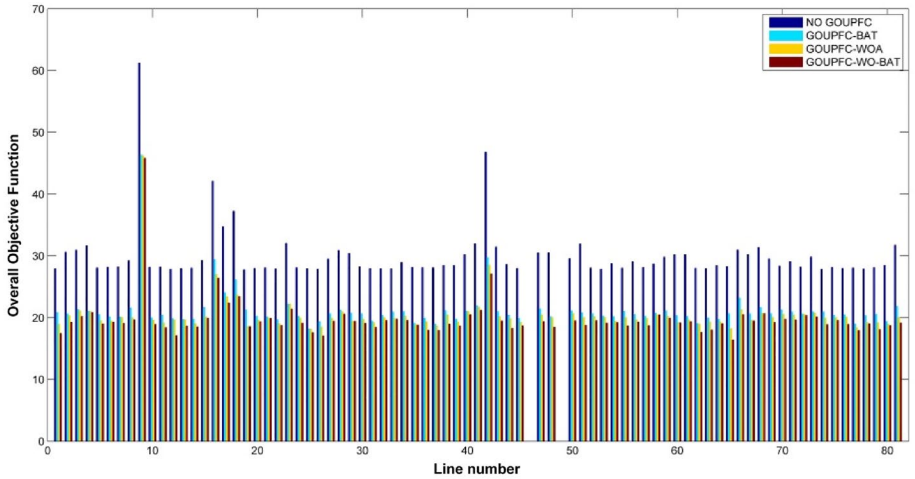

Fig. 8 GOUPFC performance under single line contingency and 30% RES

The control parameters of GOUPFC device are UPFC voltages (($r_{1\text{upfc}}$ (p.u), $r_{2\text{upfc}}$ (p.u)) and UPFC phase angles ($\gamma_{1\text{upfc}}$ (radians), $\gamma_{2\text{upfc}}$ (radians)), PST ratios ($k_{1\text{pst}}$ (p.u), $k_{2\text{pst}}$ (p.u)) and PST angles ($\sigma_{1\text{pst}}$(radians), $\sigma_{2\text{pst}}$(radians)) for IEEE-57 bus system is optimized with WO-BAT algorithm and the corresponding parameters in case 5 is presented in Table 6. Furthermore, the comparison of convergence time for the three algorithms is given in Table 7. From this table, it can be observed that the hybrid WO-BAT algorithm is converged much faster than the individual WOA and BAT algorithms in all the case studies.

Figure 10 shows the voltage profile at all the buses of IEEE-57 bus under with and without contingency conditions for base case, only with GOUPFC device and due to the presence of both GOUPFC and 50% RES support. From this figure, it is clear that the voltage profile has been improved much with GOUPFC than base case and GOUPFC with RES support than only GOUPFC device present in the system. From the above, it is concluded that the proposed GOUPFC device can improve the voltage stability not only under normal conditions but also under single line contingencies.

As the methodology is implemented on Standard IEEE 57-bus test system, and a significant improvement is observed in all the cases, we believe that this methodology also works on other networks. However, the computational efficiency of any algorithm may not quantifiable only on limited search space with small test systems. Thus, there is a need for evaluating the performance of proposed methodology on larger test systems, which we can consider as our future research work.

Conclusion

The detailed power injection modeling of the proposed FACTS device GOUPFC is presented in this paper. The optimal location of GOUPFC device is determined based on LCPI value. The performance indices and OOF value have been evaluated for different

Table 5 GOUPFC under single line contingency conditions with 0.5 RES

Line contingency	AVD			PLOSS			$LCPI_{avg}$			OOF		
	BAT	WOA	WO-BAT	BAT	WOA	WO-BAT	BAT	WOA	WO-BAT	BAT	WOA	WO-BAT
–	0.0085	0.0036	0.0031	16.1146	14.8872	14.1166	0.0616	0.0570	0.0566	16.1847	14.9478	14.1763
38–49	0.0095	0.0072	0.0015	16.9983	16.1851	15.8523	0.0613	0.0557	0.0541	17.0691	16.248	15.9079
54–55	0.0041	0.0034	0.0009	16.2212	15.8980	15.2089	0.0547	0.0538	0.0506	16.28	15.9552	15.2604
30–31	0.0070	0.0069	0.0025	16.3144	16.0271	15.8782	0.0596	0.0554	0.0545	16.381	16.0894	15.9352
37–38	0.0105	0.0071	0.0071	17.7621	16.3370	15.6785	0.0762	0.0719	0.0616	17.8488	16.416	15.7472
53–54	0.0112	0.0059	0.0025	15.8741	15.6070	15.3534	0.0665	0.0633	0.0504	15.9518	15.6762	15.4063
50–51	0.0111	0.0058	0.0050	16.9428	16.6313	16.0376	0.0589	0.0582	0.0573	17.0128	16.6953	16.0999
46–47	0.0101	0.0075	0.0025	17.6003	17.0271	15.4511	0.0653	0.0600	0.0597	17.6757	17.0946	15.5133
41–42	0.0091	0.0062	0.0021	17.7065	16.4015	15.3100	0.0624	0.0622	0.0533	17.778	16.4699	15.3654
18–19	0.0051	0.0028	0.0021	16.9446	15.8796	14.6927	0.0639	0.0499	0.0484	17.0136	15.9323	14.7432
25–30	0.0135	0.0129	0.0090	17.5112	16.8358	16.6044	0.0730	0.0647	0.0616	17.5977	16.9134	16.675

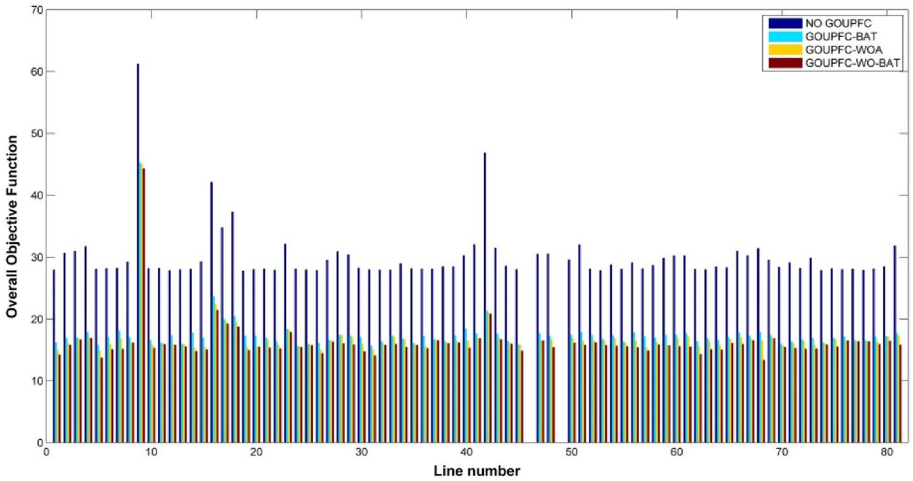

Fig. 9 GOUPFC performance under single contingency and 50% RES

Table 6 Control parameters of GOUPFC under single line contingency and 0.5 RES

Line contingency	WO-BAT							
	r_{1upfc} (p.u)	r_{2uupfc} (p.u)	k_{1pst} (p.u)	k_{2pst} (p.u)	γ_{1upfc} (rad)	γ_{2upfc} (rad)	α_{1pst} (rad)	α_{1pst} (rad)
–	0.1510	0.1904	1.0382	0.9500	− 1.6280	1.1795	− 0.3053	− 0.3075
54–55	0.1951	0.0215	0.9962	1.0392	− 0.9752	− 2.2172	0.2221	− 0.5909
30–31	0.1631	0.0223	1.0079	0.9992	− 0.1561	3.1416	− 0.4217	0.7306
37–38	0.0339	0.0264	1.0388	1.0313	− 3.1416	0.8446	0.1943	− 0.2600
53–54	0.1612	0.1119	0.9833	0.9744	− 1.1170	0.1753	− 0.4000	− 0.5196
50–51	0.1748	0.1077	1.0236	1.0088	3.1416	2.1380	0.5163	0.6649
46–47	0.0450	0.0807	0.9590	1.0500	3.0767	1.2810	− 0.6290	0.3736
41–42	0.1224	0.1337	0.9802	0.9773	− 0.2878	1.6027	− 0.0494	0.7854
18–19	0.2000	0.0122	1.0500	1.0500	− 2.7006	1.4835	0.6210	0.3872
25–30	0.1520	0.0772	1.0261	1.0142	− 0.1200	2.0976	0.7243	− 0.4862
38–48	0.0795	0.1297	0.9630	1.0375	− 1.2780	1.9343	− 0.3627	− 0.6203

Table 7 Comparison convergence time (s) for three algorithms

Line contingency	Convergence time (s)		
	BAT	WOA	WO-BAT
–	16.864	14.091	11.170
38–49	17.196	14.573	13.410
54–55	17.471	15.884	13.741
30–31	18.716	16.467	12.540
37–38	17.823	15.482	11.112
53–54	17.485	16.214	12.404
50–51	17.514	16.605	10.707
46–47	17.962	15.322	13.750
41–42	18.921	16.529	13.829
18–19	18.837	17.815	12.737
25–30	16.653	15.044	11.646

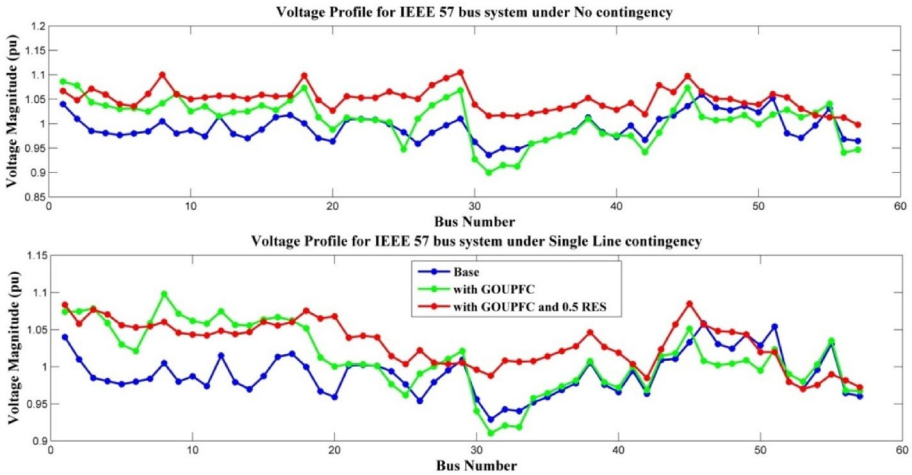

Fig. 10 Voltage profiles with and without GOUPFC and 50% RES under no/single line contingency

case studies by considering GOUPFC device at different RES penetrations. The parameters of GOUPFC are optimized by using WO-BAT, WOA and BAT algorithms. With the combination of GOUPFC and increased RES penetrations the AVDI, losses, $LCPI_{avg}$ and OOF values are considerably reduced under no contingency conditions is observed in case 1. Under single line contingency conditions, without RES and GOUPFC, there is an increment in losses, LCPI index and reduced voltage profile is observed in case 2. All the performance indices and OOF value are significantly reduced with optimal placement of GOUPFC and additional support of RES penetrations 0%, 30% and 50% in the cases 3, 4 and 5, respectively. In addition, the voltage profile is also improved for the case GOUPFC with 50% RES level when compared to the other cases. From the simulation results, the hybrid algorithm WO-BAT is performed better than the individual algorithms such as WOA-BAT in minimizing AVDI, P_{loss}, LCPI and OOF value. With the optimal location of GOUPFC, the overall system voltage profile is enhanced in IEEE-57 bus test system. Further, the impact the proposed device can be extended for large-scale systems in the real-time scenario by incorporating two or more GOUPFC devices at optimal locations which is considered as the future scope of the present work.

Abbreviations

FACTS	Flexible AC transmission systems
OUPFC	Optimal unified power flow controller
GOUPFC	Generalized optimal unified power flow controller
WO-BAT	Whale optimization-BAT
LCPI	Line collapse point indicator
RES	Renewable energy sources

Acknowledgements
Not applicable.

Author contributions
KVKK carried out the literature survey and participated in determining the modeling and optimal location of GOUPFC based on voltage collapse point indicator (LCPI). KVKK and KNVST participated in study on the different nature-inspired algorithms and among those WO-BAT, WOA and BAT algorithms are considered for this paper. KVKK and VJ carried the simulations under single line contingency conditions with the support of different RES penetrations and GOUPFC. KVKK, KNVST and VJ participated in the sequence of alignment and drafted the manuscript. All together read and approved the final manuscript.

Funding
The authors have no funding source.

Availability of data and materials
The authors of the papers used the data available at the below reference. R. D. Zimmerman, C. E. Murillo-Sanchez, and R. J. Thomas. (2011), "MATPOWER: Steady-State Operations, Planning and Analysis Tools for Power System Research and Education," IEEE Transactions on Power Systems, Vol. 26, No. 1, pp. 12–19.

Declarations

Competing interests
Modeling and Optimal location of Generalized Optimal Unified Power Flow Controller (GOUPFC) is proposed based on Line Collapse Point Indicator. WO-BAT hybrid algorithm is used for solving the complex and multi-objective optimization problem. Simulations are analysed for different RES penetration levels such as 0, 30% and 50% and GOUPFC device under single line contingency conditions. The effectiveness of the WO-BAT approach for solving the OPF problem including GOUPFC is illustrated using standard IEEE 57-bus systems and compared with WOA and BAT algorithms.

Received: 22 January 2021 Accepted: 23 July 2022
Published online: 11 August 2022

References

1. Ghiasi M (2019) Technical and economic evaluation of power quality performance using FACTS devices considering renewable generations. Renew Energy Focus 29:49–62. https://doi.org/10.1016/j.ref.2019.02.006
2. Ghiasi M (2019) Detailed study, multi-objective optimization, and design of an AC-DC smart microgrid with hybrid renewable energy resources. Energy 169:496–507. https://doi.org/10.1016/j.energy.2018.12.083
3. Kalair A, Abas N, Kalair AR, Saleem Z, Khan N (2017) Review of harmonic analysis, modelling and mitigation techniques. Renew Sustain Energy Rev 78:1152–1187. https://doi.org/10.1016/j.rser.2017.04.121
4. Barrios-Martínez E, Ángeles-Camacho C (2017) Technical comparison of FACTS controllers in parallel connection. J Appl Res Technol 15(1):36–44. https://doi.org/10.1016/j.jart.2017.01.001
5. Gaur D, Mathew L (2018) Optimal placement of FACTS devices using optimization techniques: a review. IOP Conf Ser Mater Sci Eng 331:012023. https://doi.org/10.1088/1757-899x/331/1/012023
6. Hingorani NG, Gyugyi L (2000) Understanding FACTS: concepts and technology of flexible AC transmission systems. Online ISBN: 9780470546802. https://ieeexplore.ieee.org/servlet/opac?Bknumber=5264253
7. Zhang X-P, Handschin E, Yao M (2001) Modeling of the generalized unified power flow controller (GUPFC) in a nonlinear interior point OPF. IEEE Trans Power Syst 16(3):367–373. https://doi.org/10.1109/59.932270
8. Zarrabian VS (2019) Hybrid analysis for damping inter-area oscillations using GUPFC in power systems. In: IEEE Power and Energy Society General Meeting (PESGM), Atlanta, GA, USA, pp 1–5. https://doi.org/10.1109/PESGM40551.2019.8974075
9. Shirazi AN, Mozaffari B, Soleymani S (2019) Transient stability improvement with neuro-fuzzy control of GUPFC in multi machine system. J Intell Fuzzy Syst 37:1–13. https://doi.org/10.3233/JIFS-171488
10. Sharma S, Vadhera S (2019) Development of generalized unified power flow controller (GUPFC) detailed model with a comparison with multi-UPFC. J Inf Opt Sci 40(2):233–246. https://doi.org/10.1080/02522667.2019.1578086
11. Abasi M, Joorabian M, Saffarian A et al (2020) Accurate simulation and modeling of the control system and the power electronics of a 72-pulse VSC-based generalized unified power flow controller (GUPFC). Electr Eng 102:1795–1819. https://doi.org/10.1007/s00202-020-00993-w
12. Kumar A, Sekhar C (2012) Congestion management based on demand management and impact of GUPFC. In: International conference on power, signals, controls and computation, Thrissur, Kerala, pp 1–6. https://doi.org/10.1109/EPSCICON.2012.6175244
13. Mulya Pambudy MM, Hadi SP, Ali HR (2014) Flower pollination algorithm for optimal control in multi-machine system with GUPFC. In: 6th International conference on information technology and electrical engineering (ICITEE), Yogyakarta, pp 1–6. https://doi.org/10.1109/ICITEED.2014.7007937
14. Youcef B, Ahmed A (2015) Coordinated action of OLTC and D-GUPFC for managing the distribution system voltage with DG units. In: 3rd International renewable and sustainable energy conference (IRSEC), Marrakech, pp 1–6. https://doi.org/10.1109/IRSEC.2015.7454995
15. Balusu SR, Janaswamy LN (2018) Enhancement of ATC using PSO by incorporating generalized unified power flow controller. Artif Intell Evolut Comput Eng Syst. https://doi.org/10.1007/978-981-10-7868-2_54
16. Varghese D, Janamala V (2017) Optimal location and parameters of GUPFC for transmission loss minimization using PSO algorithm. In: Innovations in power and advanced computing technologies (i-PACT), Vellore, pp 1–6. https://doi.org/10.1109/IPACT.2017.8245046
17. Nabavi Niaki SA (2002) A novel steady-state model and principles of operation of phase-shifting transformer comparable with FACTS new devices. In: Proceedings of international conference on power system technology (n.d.). https://doi.org/10.1109/icpst.2002.1067770
18. Lashkar Ara A, Kazemi A, Nabavi Niaki SA (2011) Modelling of Optimal Unified Power Flow Controller (OUPFC) for optimal steady-state performance of power systems. Energy Convers Manag 52(2):1325–1333. https://doi.org/10.1016/j.enconman.2010.09.030
19. Balachennaiah P, Nagendra P (2017) Firefly algorithm based multi-objective optimization using OUPFC in a power system. In: TENCON 2017—2017 IEEE region 10 conference. https://doi.org/10.1109/tencon.2017.8228357

20. Hosseini-Biyouki MM, Jashfar S, Vahidi B, Askarian-Abyaneh H (2017) Impact of optimal unified power flow controller in electrical transmission systems in reducing transmission cost. Electr Power Compon Syst 45(16):1762–1772. https://doi.org/10.1080/15325008.2017.1377785
21. Moazzami M, Morshed MJ, Fekih A (2016) A new optimal unified power flow controller placement and load shedding coordination approach using the Hybrid Imperialist Competitive Algorithm-Pattern Search method for voltage collapse prevention in power system. Int J Electr Power Energy Syst 79:263–274. https://doi.org/10.1016/j.ijepes.2016.01.022
22. Ara AL, Aghaei J, Alaleh M, Barati H (2013) Contingency-based optimal placement of Optimal Unified Power Flow Controller (OUPFC) in electrical energy transmission systems. Sci Iran 20(3):778–785. https://doi.org/10.1016/j.scient.2013.04.007
23. Kumar Kavuturu KV, Narasimham PVRL (2020) Multi-objective economic operation of modern power system considering weather variability using adaptive cuckoo search algorithm. J Electr Syst Inf Technol 7:11. https://doi.org/10.1186/s43067-020-00019-2
24. Kumar Kavuturu KV (2020) Narasimham PVRL (2020) Transmission security enhancement under (N—1) contingency conditions with optimal unified power flow controller and renewable energy sources generation. J Electr Eng Technol 15:1617–1630. https://doi.org/10.1007/s42835-020-00468-9
25. Tiwari R, Niazi KR, Gupta V (2012) Line collapse proximity index for prediction of voltage collapse in power systems. Int J Electr Power Energy Syst 41(1):105–111. https://doi.org/10.1016/j.ijepes.2012.03.022
26. Mirjalili S, Lewis A (2016) The whale optimization algorithm. Adv Eng Softw 95:51–67. https://doi.org/10.1016/j.advengsoft.2016.01.008
27. Watkins WA, Schevill WE (1979) Aerial observation of feeding behavior in four baleen whales: Eubalaena glacialis, Balaenoptera borealis, Megaptera novaeangliae, and Balaenoptera physalus. J Mammal 60(1):155–163. https://doi.org/10.2307/1379766
28. Yang X, Hossein Gandomi A (2012) Bat algorithm: a novel approach for global engineering optimization. Eng Comput 29(5):464–483. https://doi.org/10.1108/02644401211235834
29. Zimmerman RD, Murillo-Sánchez CE, Thomas RJ (2011) MATPOWER: steady-state operations, planning, and analysis tools for power systems research and education. IEEE Trans Power Syst 26(1):12–19. https://doi.org/10.1109/tpwrs.2010.2051168

Publisher's Note